Title

A New Wideband Spread Target Maximum Likelihood Estimator for Blood Velocity Estimation: Part Two - Evaluation of Estimators with Experimental Data

Journal

IEEE Transactions on Ultrasonics, Ferroelectrics and Frequency Control, 38

Authors

Ferrara, K. Whittaker
Algazi, Ralph

Publication Date

1991

Peer reviewed

T-UFFC/38/1//40245

A New Wideband Spread Target Maximum Likelihood Estimator for Blood Velocity Estimation Part II: Evaluation of Estimators with Experimental Data

Katherine W. Ferrara
V. Ralph Algazi

Reprinted from
IEEE TRANSACTIONS ON ULTRASONICS, FERROELECTRICS, AND FREQUENCY CONTROL
Vol. 38, No. 1, January 1991

A New Wideband Spread Target Maximum Likelihood Estimator for Blood Velocity Estimation—Part II: Evaluation of Estimators with Experimental Data

Katherine W. Ferrara, *Member, IEEE*, and V. Ralph Algazi, *Senior Member, IEEE*

Abstract—**Part I of the work presented the derivation and theoretical evaluation of new wideband maximum likelihood strategies for the estimation of blood velocity using acoustic signals. In Part II, the signal models and performance of the estimation strategies described in Part I are tested with experimental ultrasonic data. The ultrasonic data analyzed in the work verifies the theoretical model and predicted performance. The averaged correlation, verified experimentally, confirms that the correlation envelope can be used to estimate the velocity of scatterers, and that the shape of the correlation function conveys information regarding the velocity profile within the sample volume. For both the wideband point and range spread estimators, the predicted improvement in velocity resolution and the reduction in the height of subsidiary velocity peaks are demonstrated. Through the use of these estimation strategies, information regarding the mean velocity and velocity variation are available for each spatial location within the vessel. This information is presented using a three-dimensional (3-D) spatial velocity profile display, which appears to offer a number of advantages in the rapid identification of pathology.**

I. Introduction

PART I of this work presented the theoretical derivation and analysis of the wideband maximum likelihood estimators. A new wideband range spread maximum likelihood estimator and a simpler wideband point target MLE were analyzed and evaluated. These estimators utilize both the change in scatterer position and the change in frequency of the returned signal to estimate the velocity distribution of the blood scatterers. Theoretical performance improvements, possible with these new strategies, were shown through improved local and global accuracy of the estimators. The performance of the estimation strategies described in Part I [9] is experimentally confirmed using ultrasonic data. This experimental evaluation is reported in the second part of the paper.

First, we evaluate the statistics and properties of the experimental data and confirm that the model in Part I [9] accurately describes the received signal for the acoustic environment. As predicted, the mean scatterer velocity and the presence of a velocity spread target affect the magnitude and periodicity of the autocorrelation, as well as the phase.

Second, we demonstrate that the experimental performance of the wideband maximum likelihood estimator is accurately predicted by the expected estimator output computed in Part I. Thus, using the wideband MLE, we will show that the velocity resolution is improved, and that the height of subsidiary velocity peaks is markedly reduced in comparison with current commercial strategies.

In our comparative study, the experimental performance of the wideband MLE is evaluated and compared to the performance of the classical narrowband MLE and to the theoretical predictions from Part I. In order to evaluate the potential for spatial-velocity mapping, a wideband transmitted signal is used in this analysis.

The theoretical model used in Part I assumes the amplitude of the received signal from blood scatterers to be random and to be statistically independent for separate regions of scatterers. Since the wideband MLE can track these scatterers using their returned amplitude and a moving sample volume, it achieves superior performance. Comparison of the wideband MLE with a narrowband MLE, which uses a fixed sample volume therefore provides a basis for evaluation of the effectiveness of the "tracking" of the wideband MLE. In addition, it provides the opportunity to verify the assumptions of the theoretical model through the use of experimental data.

Third, we confirm that these new estimation strategies result in a more effective use of the available data. We consider several important time intervals that include the *axial* window, defined as the temporal window applied to data from a single *A* line, the *data* window, defined as the window applied to the data from multiple vectors used in computing a single estimate, and the *observation* window, defined as the window applied to subsequent estimates in the computation of an averaged estimate. The effect of the length of the data window, the use of statistical estimator averaging, and the effect of the length of the observation window are evaluated.

Finally, a new three-dimensional (3-D) method of spatial-velocity profile display is introduced. This method appears to offer a number of advantages in the rapid identification of pathology.

Section II describes the parameters of the data used and the signal processing structures used in processing the raw rf data. In Section III the statistics of the received data are computed and the periodicity of the envelope of the received signal is

Manuscript received July 3, 1989; revised July 13, 1990; accepted July 16, 1990.

K. W. Ferrara is with the Department of Electrical and Electronic Engineering, California State University, Sacramento, CA 95819, and with the Center for Image Processing and Integrated Computing (CIPIC), University of California, Davis, Davis, CA 95616.

V. R. Algazi is with the Center for Image Processing and Integrated Computing (CIPIC) and with the Department of Electrical Engineering and Computer Science, University of California, Davis, Davis, CA 95616.

IEEE Log Number 9040245.

shown to change with the velocity of the scatterer, as predicted. Section IV shows that the experimental velocity resolution, as measured by the width of the mainlobe of the estimator output, was accurately predicted by the theoretical expected receiver output. In Section V the predicted decrease in the height of the subsidiary velocity peaks is demonstrated in the acoustic data. Section VI demonstrates that the change in the relative magnitude and shape of the velocity distribution occurs as predicted by the theoretical model, and illustrates the additional information that is contained in the velocity distribution at each spatial location. Section VII demonstrates the superiority of the wideband estimation strategies in the spatial mapping of velocity components through the use of 3-D spatial-velocity plots. Section VIII presents a comparison of the performance of various *mean* velocity estimators, and a brief concluding section ends the paper.

II. Characteristics of the Data and Preprocessing Schemes

A. Data

The ultrasonic data used within this paper demonstrates the behavior of fluids with a high volume concentration of scatterers moving through a straight tube at a nonzero beam vessel angle. The scatterers are moving at a relatively slow velocity. This situation can be used to illustrate a number of features of various estimators, as well as features of the theoretical model.

The data set was collected by Paul Embree and was also used in Embree [1]. The data consists of acoustic echos from Sephadex G-10 particles travelling within a 50% glycerin-water solution in a straight plastic tube. The transducer excitation approximated an impulse, and the received bandwidth was approximately 2 MHz. The transducer focal point was located at the midpoint of the vessel. The data from the transducer was amplified and then the RF waveform was immediately digitized. The parameters of the data collection system were given as follows.

Transducer center frequency	5 MHz
RF sampling rate	50 MHz
Pulse repetition frequency	7812.5 Hz
Range gate delay	54.35 us
Transducer 3-dB bandwidth	2.5 MHz
Tube diameter	7 mm
Ultrasonic measurement angle	45 degrees
Volume flow rate	281 ml/min
A line length (1024 samples)	20.48 us
Acoustic velocity	1500 m/s
Ampifier Bandwidth	40 MHz

Using a parabolic flow assumption, the peak midstream velocity is 0.243 m/s. The z component of this velocity would then be 0.172 m/s. This produces a peak time shift between A lines of 29.4 ns. The peak doppler shift is 1147 Hz. Using a 0.8-mm 3-dB beamwidth in the focal zone and peak radial velocity of 0.172 m/s, the transit time of the highest velocity scatterers is approximately 4.65 ms or 36 periods at the pulse repetition frequency of 7812.5 Hz. The effective transit time through the *entire* beam width is slightly larger.

Fig. 1 shows the expected axial velocity component for each radial vessel coordinate. The lateral size of the sample volume is fixed by the beam width and approximated by the ultrasonic beam in Fig. 1. The axial sample volume size is determined by the transmitted burst length and the data window used for each estimate, due to the axial tracking of the estimator. By observing the velocity components present at each spatial location, this figure shows that increasing the number of periods or sample volume size increases the axial velocity gradient contained in each spatial estimate of the received signal. The choice of the data window (number of periods used for a single estimate) should therefore be considered carefully.

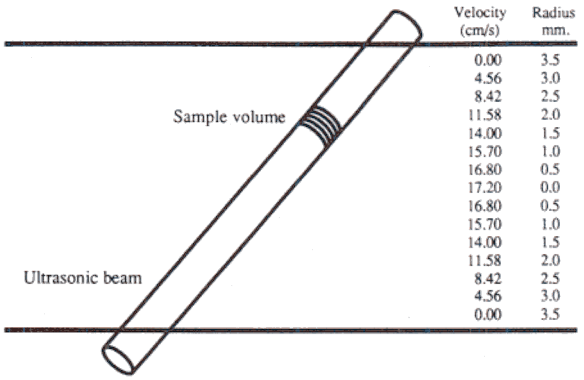

Fig. 1. Relationship of ultrasonic beam and vessel

The data displayed in the later sections of this paper is indexed as follows. The depth, or range, of a sample varies from 0-1023 along the beam axis. This index represents the starting position of the sample volume for the first pulse. The first vessel wall occurs at approximately sample 280 in this filtered data set. The final vessel wall begins at approximately sample 910. It is important to recognize that the amplitude of the return from the vessel wall is much larger than the return from surrounding areas. Therefore, due to the width of the beam in the lateral dimension, the scattered energy from the vessel wall affects samples corresponding to a range of axial positions.

B. Implementation of Signal Preprocessing Schemes

Baseband signal processing techniques were used in the preprocessing of the data. In order to reduce unwanted noise, the data was first low pass filtered, using a 29-point FIR low pass filter with a 3-dB cutoff point of 9 MHz. The data was then multiplied by a complex exponential signal of 5 MHz. Finally, the data was again low pass filtered using a 31 point FIR low pass filter with a 3-dB bandwidth of 3 MHz.

III. Computed Statistics of the Data

In order to determine the accuracy of the theoretical model, the mean and time averaged correlation of the data are computed and compared to the mean and autocorrelation predicted in Part I. To illustrate the effect of the velocity on the received signal, the correlation for two spatial regions is calculated and studied as a function of the change in the delay of the received signal and the number of periods between samples.

First, we observe that the data has zero mean as expected.

Next, we consider the correlation and note that the delay of the received signal from a group of moving scatterers is expected to change by $mT(2v/c)$, where m represents the number of periods between samples, T represents the transmitted pulse repetition period, v represents the scatterer velocity and c represents the acoustic velocity. The correlation between the signal arriving after a delay of time t_o and the signal arriving after a delay $t_o + \tau + mT$ is therefore studied as a function of τ and m. In Part I, it was shown that the maximum correlation should occur for $\tau = mT(2v/c)$, and therefore the peak of the correlation can be used to estimate the velocity v.

The correlation computed before averaging is given by

$$C_k(t_o, t_o + \tau; m) = \int_{-\infty}^{\infty} r_k(t + t_o)a(t + t_o)$$
$$\cdot_m(t + t_o + \tau)a(t + t_o + \tau)\, dt$$

where $r_k(t)$ is the return from the kth pulse, $a(t)$ represents the axial window, and t_o is a temporal offset where $0 < t_o < T$. The axial window used in this case was a rectangular window of length equivalent to six times the acoustic wavelength. Axial windows of four to six times the acoustic wavelength generally produced the best results, maximizing the correlation and minimizing the noise.

In order to evaluate the time averaged properties of this quantity, the magnitude of $C_k(t_o, t_o + \tau; m)$ can be averaged over all original vectors k. Let $C(t_o, t_o + \tau; m)$ represent the averaged quantity. These quantities are normalized by the averaged correlation at lag zero near the center of the vessel, $C(t_1, t_1; 0)$, where t_1 corresponds to the signal travel time to a sample volume that initially is approximately centered in the vessel (sample 600). At this position the velocity of the scatterers within the sample volume is nearly uniform. The normalized quantity is plotted in Figs. 2–4.

Fig. 2 shows a 3-D plot of the normalized averaged correlation for data from the center of the vessel, $C(t_1, t_1 + \tau; m)/C(t_1, t_1; 0)$ using various values of m and τ. Fig. 3 shows the correlation at this position before averaging over the data set, $C_1(t_1, t_1 + \tau; m)/C(t_1, t_1; 0)$. In each figure, we observe that the *location of the peak of subsequent periods* of the correlation is shifted by the target velocity. Since the maximum correlation should occur for $\tau = mT(2v/c)$, in this region for uniform velocity denoted by v, we expect the correlation peak to be a linear function of τ/m. Using the three dimensional plot, we see that the projection of these peak locations into the 2-D τ-m plane is, as expected, a straight line. For a range of values of m, both the single calculation results and the averaged correlation using the slope of this line show a peak corresponding to an identical velocity of 0.15 m/s. This is quite close to the experimental result of Embree. He predicted a peak velocity of 0.172 m/s in the center of the vessel, which would produce a mean velocity for this position of approximately 0.16 m/s.

An evaluation of the peak of the averaged correlation of the signal at this axial position, with its nearly uniform scatterer velocity, shows that the *peak* in Fig. 2 accurately predicts the scatterer velocity for a maximum lag of 46 transmitted periods, or equivalently, as the scatterers move approximately 1 mm across the beam width. In Fig. 3 additional peaks occur, and the maximum correlation accurately predicts the velocity of the scatterers for a maximum lag of 25 periods.

In both figures, the *magnitude* of the peak of the correlation decreases as a function of m. This is expected, because of the 45-degree beam vessel angle and therefore the movement of scatterers across the lateral beam dimension. The predicted decrease in the peak of the autocorrelation for a scatterer velocity of 0.16 m/s and a 45 degree beam vessel angle was computed. This decrease closely matches the computed value for the experimental data.

Without averaging, the correlation of the received signal is noisy and displays additional peaks as well as the expected peak. In order to use the magnitude of the correlation function as an estimate of velocity, $C_k(t_o, t_o + \tau; m)$ must be computed and should be averaged over k. Optimally the average would in-

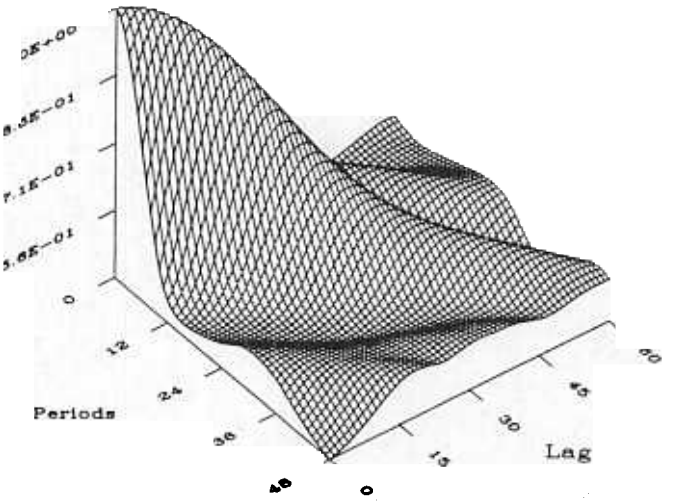

Fig. 2. Normalized averaged correlation, $C(t_1, t_1 + \tau; m)/C(t_1, t_1; 0)$, of data from location 600, using the period index m, and lag τ indexed by 20 ns samples.

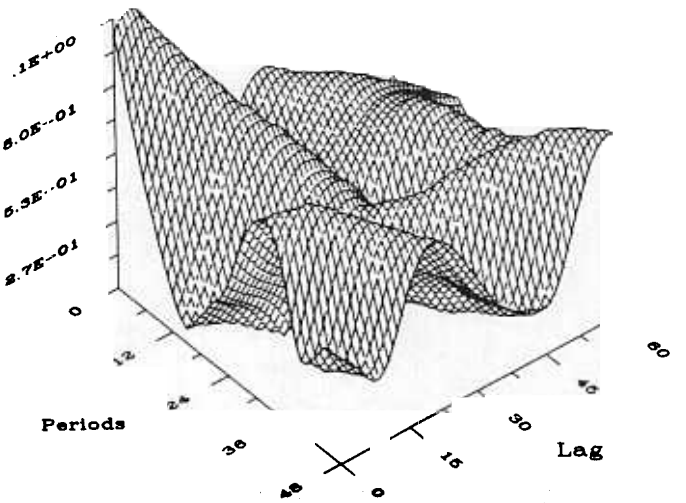

Fig. 3. Normalized correlation, $C_1(t_1, t_1 + \tau; m)/C(t_1, t_1; 0)$, of data from location 600, using the period index m, and lag τ indexed by 20 ns samples.

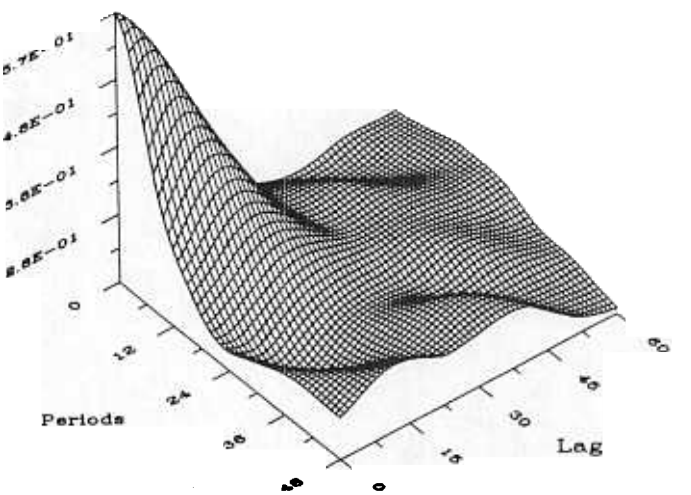

Fig. 4. Normalized averaged correlation, $C(t_2, t_2 + \tau; m)/C(t_1, t_1; 0)$, of data from location 400, using the period index m, and lag τ indexed by 20 ns samples.

clude all received data that corresponds to stationary statistics. As the blood flow accelerates, the mean velocity cannot be considered stationary, and therefore a maximum estimation interval exists.

Velocity Spread Target: In Fig. 4, the normalized average correlation $C(t_2, t_2 + \tau; m)/C(t_1, t_1; 0)$ is displayed for a different value of the temporal offset, t_2. This offset corresponds to a volume of scatterers at position 400, which contains a velocity spread target. The peak of the correlation corresponds to a velocity of 0.09 m/s, which accurately matches the expected mean velocity within the sample volume.

As predicted in Part I, we observe that the shape of the autocorrelation is affected by the width of the velocity distribution within the sample volume. The peak of the correlation function decreases more rapidly as a function of m when a velocity spread target is present. In this region of velocity spread (Fig. 4), the averaged correlation can be used to predict the scatterer velocity for a lag that is less than 32 transmitted periods. This compares to 46 periods in the absence of velocity spread (Fig. 2). This decrease was predicted by the model for the statistics of the received signal.

Also of interest in this example is the correlation at lag zero, denoted $C(t_o, t_o; 0)$. The magnitude of the time averaged correlation at lag zero is larger in the center of the vessel. Since the transducer focus was centered within the vessel, a decrease in the beam magnitude at other locations is expected. The far field decrease can be predicted (using the method discussed by Azimi and Kak [2]), and reduced using a transducer with a dynamic focal depth. In this case, the computed decrease was slightly larger than the predicted value. Although turbulence was not present under these experimental conditions, several researchers have reported a decrease in the time averaged value of $C(t_o, t_o; 0)$ in the presence of turbulence [4]–[6]. We wish to emphasize that when using the wideband MLE, with its superior spatial resolution, the potential exists for further research into the spatial mapping of the properties of blood in the presence of velocity gradients and turbulence.

The correlation at multiples of the transmitted pulse repetition period denoted by $C(t_o, t_o; m)$ corresponds to the $\tau = 0$ axis in Figs. 2–4 and can be studied as a function of m. The correlation of the data at these integer values of the transmitted period decreases substantially with an increase in m or an increase in the scatterer velocity, as predicted in Part I. In fact, we observe that the correlation is determined by the baseline noise level after ten periods. This situation corresponds to narrowband estimation that does not track the scattering medium and could therefore utilize a very limited number of correlated data values.

Conclusion of the Statistical Analysis of the Data: The predicted changes in the autocorrelation of the received signal have been verified using the time averaged correlation of experimental acoustic data. The *location of the peak of subsequent periods* of the correlation is shifted by the target velocity. In addition, the *magnitude and shape of the peak of subsequent periods* of the correlation is strongly affected by the width of the velocity distribution within the sample volume.

IV. Comparison of the Expected and Experimental Estimator Outputs

In this section, the expected estimator output, evaluated using the expressions derived in Part I, is compared with the estimator output computed from ultrasonic data. In evaluating the expected estimator output, the model for velocity variation includes the portion of the parabolic distribution expected in each spatial location. The expected receiver output derived in Part I is evaluated using a center frequency of 5-MHz, a two-cycle rectangular envelope, and a repetition frequency of 7812.5 Hz. The experimental estimator output is computed for each particular region of the vessel, with the experimental data reflecting the degree of velocity spread. The expected and experimental output are compared in terms of bias, resolution, and effect of the data and observation windows.

In any practical situation, a tradeoff exists between estimator resolution and reliability. This situation is analogous to the spectral estimation case, although here the wideband MLE estimates position *and* frequency. Due to the results for estimator resolution in Part I, it is expected that the velocity resolution of the estimator would improve with an increase in the data window. In order to improve the *reliability* of the velocity estimate, it is beneficial to average subsequent estimates. It has been reported [7] that the underlying process can be considered to be stationary up to 10 ms. After this time, at least within the arterial system, some acceleration must be considered. The total amount of data which can be used without consideration of acceleration is therefore limited.

A. Bias

The *sensitivity* is determined here by the expected receiver output for a scatterer traveling at a velocity v and a receiver also tuned to velocity v. Due to the tracking nature of the estimator, the predicted sensitivity of the *wideband* MLE output is constant for the range of scatterer velocities in the experimental data. It is therefore unbiased in the absence of frequency dependent attenuation. By contrast, the predicted sensitivity of the *narrowband* MLE decreases as a function of the scatterer velocity, because the limited transit time of higher velocity scatterers within the fixed sample volume results in a larger expected estimator output for lower velocity scatterers. Therefore, the narrowband MLE exhibits a *negative bias*. Using (36) from Part I [9], the expected output of the narrowband receiver is plotted in Fig. 5 for a data window of 40 periods.

It will be shown that the negative bias is also observed in the experimental estimator output for the narrowband MLE. The peak velocity in the center of the vessel is computed as 0.14 m/s rather than 0.16 m/s, as expected from the experimental conditions and use of other estimators.

B. Resolution—Expected and Experimental

Using (33), (36), and (37) from Part I, Fig. 6 shows the *expected* velocity *resolution* of the narrowband and wideband MLEs. The data window is 35 periods, the scatterer velocity is 0.2 m/s. The improvement in velocity resolution using the wideband estimation scheme is clear. The half amplitude width of the mainlobe for the narrowband MLE is nearly double the width of the mainlobe for the wideband point MLE. The wideband range spread MLE demonstrates additional improvement over the point estimator evaluated for a range spread target.

The *expected* likelihood function of the wideband point MLE, in the presence of a range spread target with a uniform velocity, is shown in Fig. 7 for a data window of 25–40 periods, which is assumed to be smaller than the transit time of the scatterers through the lateral beam width. Clearly, the velocity resolution of the wideband point MLE is expected to improve as the data window increases.

Experimental Resolution Obtained for the Wideband Point MLE: Using a tapered data window of 50 periods, the *experi-*

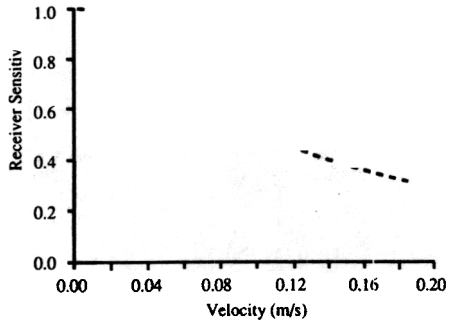

Fig. 5. Expected output of the narrowband MLE for a 40-period data window.

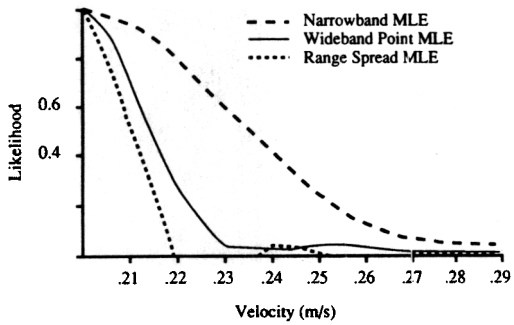

Fig. 6. Comparison of expected estimator output using parameters of experimental conditions.

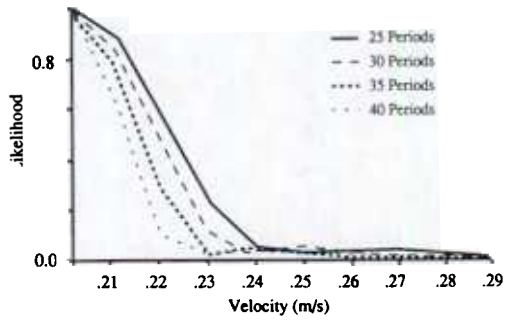

Fig Effect of data window on expected performance of the wideband point MLE.

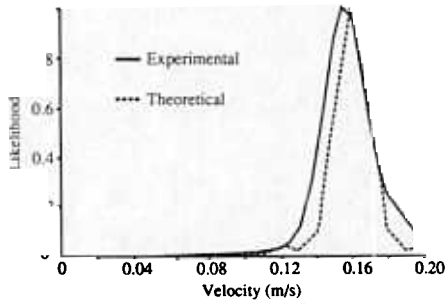

Fig. 8. Comparison of theoretical and experimental resolution of the wideband point MLE.

mental receiver output measured in the center of the vessel using the wideband point MLE was compared to the *expected* receiver output for a range spread target of velocity 0.16 m/s and is shown in Fig. 8. The experimental velocity distribution is slightly wider than the theoretical resolution of the wideband point MLE evaluated for this uniform velocity target. In this figure the presence of some scatterers with a velocity which is slightly less than 0.16 m/s is shown, as expected in this axial position.

Resolution of the Narrowband MLE: The experimental narrowband receiver output, using data from the center of the vessel and a tapered data window of 50 periods, is compared to the theoretically predicted resolution of the narrowband MLE with a uniform target velocity of 0.14 m/s in Fig. 9. Note that the lower sensitivity of the narrowband MLE produced a biased estimate. The experimental peak occurs at approximately 0.14 m/s instead of 0.16 m/s as expected from the flow parameters.

The velocity spread of the receiver output is approximately equal to the predicted spread. Since the estimate exhibits a negative bias, and therefore has a peak at 0.14 m/s, the presence of scatterers moving at 0.15–0.16 m/s widens the velocity distribution. The estimator is less sensitive to these velocity components, but a finite receiver output is produced at these velocities, and therefore the receiver output deviates from the expected distribution.

Resolution Comparison—Wideband Point MLE and Narrowband MLE: The experimental receiver output of the wideband point MLE and the narrowband MLE for scatterers in the center of the vessel is shown in Fig. 10. This comparison is made using a tapered data window of 50 periods. The wideband point MLE clearly demonstrates superior velocity resolution even for the low scatterer velocity of 0.16 m/s. Therefore, the use of scatterer "tracking" by the wideband MLE has significantly improved the velocity resolution. The narrowband half amplitude resolution is degraded from the wideband MLE by approximately a factor of two, as predicted. In addition, the bias of the narrowband MLE can be observed.

Resolution of the Wideband Range Spread MLE: The experimental receiver output of the wideband range spread MLE was computed for a raised cosine data window of 35 periods (one sided width) and signal to noise ratio of 10 dB and is shown in Fig. 11. The wideband point MLE is shown for comparison with a tapered data window of 35 periods. Due to the nature of the wideband range spread MLE, the data window must be implemented as a window over the temporal difference between two times t and u, and therefore is defined differently. The improved resolution of the range spread MLE in comparison with the wideband point MLE is apparent.

Once again this figure corresponds to illumination of the scatterers at the center of the vessel that have a nearly uniform velocity, and therefore, the experimental receiver output should be approximately equivalent to the expected estimator resolution. Comparing Figs. 6 and 11, we observe that the experimental mainlobe is slightly wider.

Resolution for a Short Data Window: The comparison of estimator performance was also made for a short data window of eight periods. The purpose of this evaluation was to determine the difference in performance between the estimators for an interval that would be used in the technology known as color flow imaging. Because of the low velocity of the scatterers and short observation interval, the difference in transit time is negligible and the resolution of the wideband point MLE and narrowband MLE, as defined in Part I, is nearly equal. However, as expected, the narrowband MLE continues to exhibit a negative bias. Also, as predicted in Part I, the local accuracy of the wideband point MLE and the narrowband MLE is nearly equivalent when the data window is less than the scatterer transit time through the axial length of the sample volume. However, at

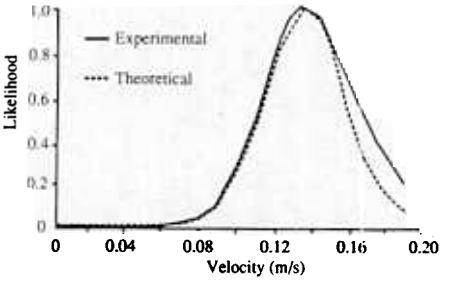

Fig. 9. Comparison of theoretical and experimental resolution of the narrowband MLE.

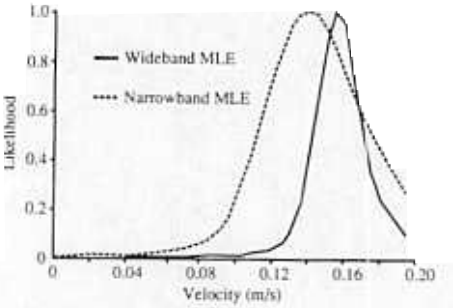

Fig. 10. Experimental comparison of wideband point MLE and narrowband MLE for a long data window.

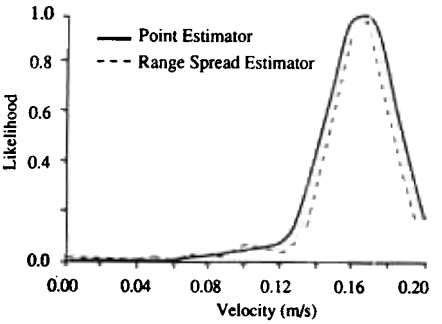

Fig. 11. Comparison of experimental resolution of wideband point and range spread MLE.

higher scatterer velocities, and when using longer data windows, the performance of the narrowband MLE is inferior.

Although not shown, the performance of a suboptimal form of the narrowband MLE that uses only the correlation at a single lag of one period has been evaluated and shows a very significant decrease in local and global accuracy. Such estimators have been proposed for color flow imaging [8].

C. Discussion Regarding Data Window Versus Resolution

One would typically expect the velocity resolution to improve with an increase in the data window, until the data window equals the transit time of the scatterers. However, the correlation of the received signal was shown to be reduced by the presence of a velocity spread target, and the optimum data window is limited by the length of the correlated signal. The improvement in velocity resolution due to an increase in the length of the data window is shown in this section to vary with the illuminated velocity distribution.

Fig. 12 shows the resolution improvement at sample position 400 (illuminating a velocity spread target), which results from increasing the data window from 30 to 40 periods. We also observe that the mean velocity is increased slightly by the increase in the data window, due to the axial velocity gradient. As the data window is increased to 50 periods, the velocity resolution does not show a significant change. Using the correlation peak to estimate the velocity of the scatterers, the maximum lag which accurately predicted the velocity at this position was approximately 32 periods. Therefore, as expected, the limited correlation of the received signal, due to the velocity distribution within the sample volume, limits the attainable resolution.

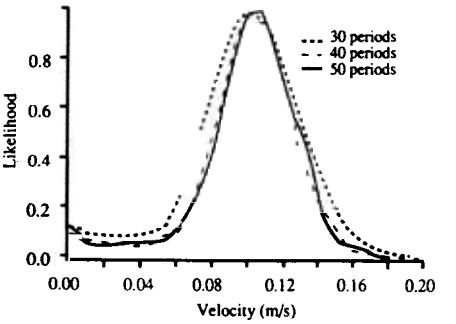

Fig. 12. Experimental output of wideband point MLE using several data windows for velocity spread target, located at index 400.

Fig. 13 shows the resolution versus data window for sample position 600, which is near the center of the vessel. The velocity within the sample volume is nearly uniform at this position, and the maximum lag for which the correlation peak accurately predicted the velocity was 46 periods. It was therefore expected that the optimal data window would be longer than the optimal window at position 400. This figure shows that the velocity resolution improves as the data window is increased from 30 to 40 and 40 to 50 periods. This important experimental result shows that the optimal data window increases when illuminating a uniform velocity target.

One of the important features of the wideband MLE is that the data window is not required to be the same for all sample volumes within the vessel. The wideband MLE allows the selection of an appropriate data window for each part of the scattering medium.

In addition, because of the transmission of a wideband signal, the axial dimension of the sample volume is small, and therefore the spatial resolution is not degraded. Scatterers are tracked in the axial dimension for a distance that corresponds to the length of the coherent signal. Therefore, at *all* axial positions, the velocity resolution can be maximized without the spatial resolution limitation of narrowband systems, imposed by the choice of an axial signal length which must be constant for all axial positions.

D. Discussion of the Data and Observation Window Versus Reliability

In the proposed strategies, the averaging of subsequent estimates increases reliability if the underlying process can be considered to be stationary, and therefore does not involve a significant acceleration. To take advantage of this property would require the investigation of the maximum time interval of underlying stationarity for blood velocity at various points within the circulatory system. Once the stationary interval is determined, the optimal observation window for the stationary data can be calculated.

Note that since the stationary interval is limited, the maximum observation window is also limited. Based upon classical estimation theory we note that for a rectangular window, a ratio of the observation window to the data window of ten or greater

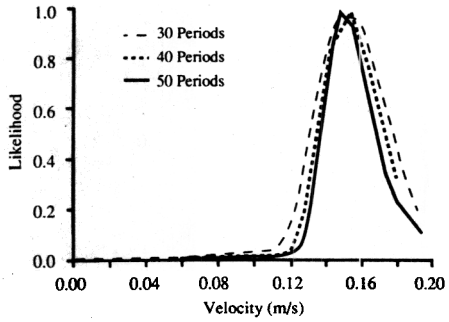

Fig. 13. Experimental output of wideband point MLE using several data windows for uniform velocity target, located at index 600.

is needed for a reliable estimate. Therefore, an increase in the data window of an individual estimate within a fixed observation window eventually results in decreased reliability.

V. Evaluation of Subsidiary Velocity Peaks

In this section, the height of the first subsidiary peak is computed for the wideband and narrowband MLEs, and it will be demonstrated *by numerical evaluation* that the subsidiary velocity peaks of the wideband MLE are significantly reduced. Since it is the statistical independence of the received signal from separate regions of scatterers that reduces the expected magnitude of the subsidiary peak, this result verifies the statistical assumptions of the theoretical model used in Part I. The assumption of independence was based upon the random initial position and random concentration variation of scatterers in adjacent regions.

In a second experiment, the data vectors are downsampled sufficiently to produce aliasing. Evaluation of the wideband and narrowband MLE with the reduced data set shows that the wideband MLE suppresses the height of the aliased velocity peak.

Wideband Point MLE: Using a data window of 35 periods, the height of the first subsidiary velocity peak was computed and occurs at the theoretically predicted location of 1.16 m/s plus the actual mean velocity. This peak reaches a maximum of 25% of the amplitude of the true peak using the wideband point MLE. In the center of the vessel the maximum subsidiary peak is 10% of the amplitude of the true peak. *The predicted suppression of aliasing effects is therefore confirmed.* Some additional peaks of similar magnitude (25% of the true peak) occur near 0.9 m/s in regions near the vessel wall. These were due to the limited axial range of the data.

To verify the reduction in aliasing, the vectors were downsampled by a factor of 10, and each estimate was based on five samples. The effective pulse repetition frequency is then 781.25 Hz. In this situation, the aliased peak occurs in the region of 0.0–0.02 m/s. This process drastically reduced the signal to noise ratio, and the estimates produced by this low signal to noise ratio were then averaged to reduce the variance. The maximum amplitude of the subsidiary velocity peak for the wideband MLE was 57% of the amplitude of the receiver output at the peak velocity. For a situation of higher SNR, an increased number of data samples per estimate, or a nonperiodic sampling scheme, this peak would be even smaller.

Wideband Range Spread MLE: The height of subsidiary velocity peaks for the complete data set was also evaluated using the range spread MLE. The results were very similar, with a maximum subsidiary peak of 20% of the true peak obtained.

Narrowband MLE: In contrast, the subsidiary peak of the narrowband MLE was equal to the height of the receiver output for the true peak velocity in both aliasing experiments. In some regions the subsidiary peak was slightly larger than the main peak. Therefore, for higher velocity scatterers the potential exists for velocity aliasing, as expected. In addition, the subsidiary peak increases the noise contained in the estimate.

From this examination of the aliased peaks, we conclude that in a moderate signal to noise condition the height of subsidiary velocity peaks is considerably reduced by the use of the wideband MLE.

VI. Receiver Output as a Function of Velocity Distribution

The velocity distribution of scatterers in two spatial locations is shown in Fig. 14. The curves show the normalized distribution near the center of the vessel (sample 600) and approximately two thirds of the distance to the vessel wall (sample 400). The receiver output for sample 400 has been normalized by the ratio of the received power in the two positions, in order to account for the transducer focal parameters.

Fig. 14 shows that the relative amplitude of the receiver output decreases near the wall of the vessel, and the width of the receiver output increases. In Section VIII, the second moment of the receiver output is computed for each spatial position and shown to increase as the illuminated velocity spread increases. As shown in Fig. 14, the integral over all velocities of the receiver output also decreases as the width of the illuminated velocity distribution increases. This can be predicted from Part One, (13), in which the receiver output was shown to be proportional to the correlation of the received signal integrated over times t and u, which decreases as the width of the velocity distribution increases.

Both the change in relative amplitude and width of the receiver output, as a function of illuminated velocity distribution, were predicted by the theoretical model, and these effects are thus verified using the experimental data. Since the theoretical resolution of the receiver for a given data window is known, by comparing the velocity distribution from the experimental receiver output at each spatial location with the resolution of the receiver, an estimate of the velocity spread of the target could be obtained. Therefore, the wideband MLE has the potential to improve estimation of the spatial variation in velocity spread as well as the estimation of the maximum likelihood velocity.

VII. 3-D Display of Spatial-Velocity Estimates

In this section, the data from a single estimate, as well as the average of all estimates within the set of data, are displayed in 3-D plots. The 3-D plots will show the receiver output for each axial spatial volume and each velocity considered. An individual estimate is made using 30–50 vectors. The data window is then shifted by fifty percent of the number of vectors used per estimate and another estimate is computed. Averaged estimates for each velocity and axial spatial position are then calculated using all 384 vectors. The two-dimensional (2-D) velocity distribution for each spatial position can then be observed, as well as the variation in the velocity across the vessel.

There are two purposes for the 3-D plots of the spatial-velocity profile. The first is to demonstrate the spatial-velocity information available with each estimator. The second purpose is to suggest an alternative display strategy for the velocity data. This method of display allows the velocity distribution for each line of sight at all axial locations to be visualized simultaneously and offers several advantages. The first is that it offers an efficient method to examine the velocity profile across an entire vessel. The frame rate and estimator quality can be maintained due to the single line of sight. Second, the 3-D display

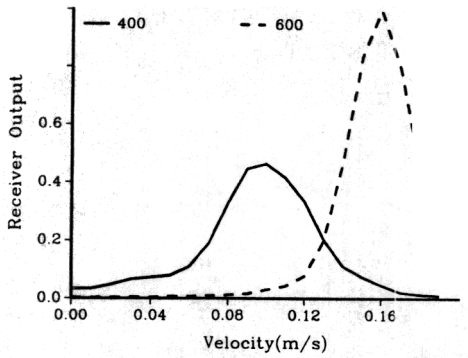

Fig. 14. Experimental output of wideband point MLE as function of velocity distribution.

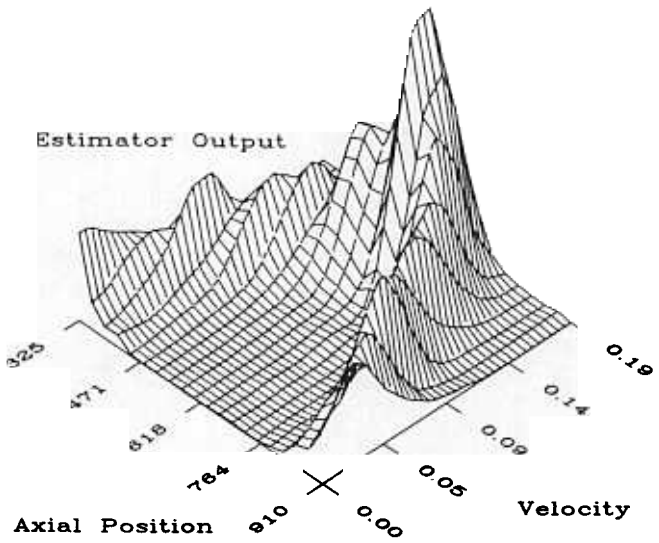

Fig. 15. Three-dimensional display of wideband point MLE, data window of 30 periods, as function of indexed axial position and velocity in m/s.

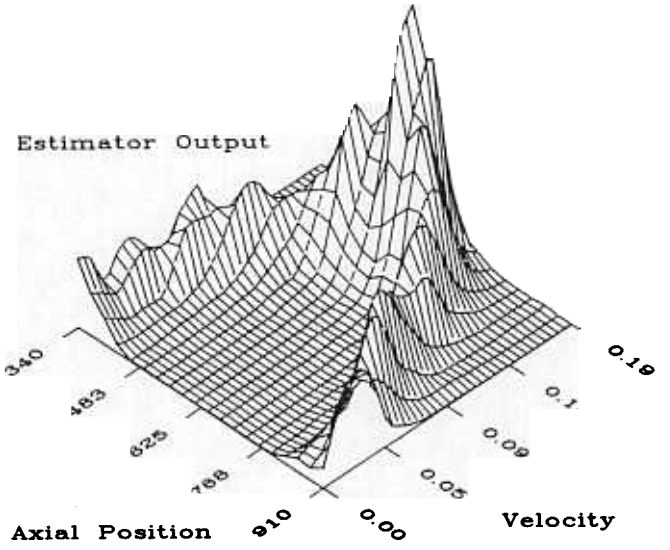

Fig. 16. Three-dimensional display of wideband point MLE, data window of 50 periods, as a function of the indexed axial position and velocity in m/s.

provides more information than the traditional 2-D Doppler spectrum. Information regarding the mean velocity and velocity distribution for each spatial location is contained in the display. The line of sight could then be swept through the vessel to identify areas of pathology. An area of stenosis would be expected to produce a narrowing of the spatial dimension, as well as a change in the maximum velocity and velocity profile, and would be efficiently shown in the three dimensional display.

A number of features of the spatial velocity field can be observed using the 3-D plots. First, the parabolic nature of the velocity distribution across the vessel can be observed. Second, the velocity distribution of the scatterers within each spatial volume can be estimated. Quantification of the effect of the velocity spread target on the amplitude of the received signal at each spatial position, when using a fixed focus transducer, would require that the effect of the transducer focal parameters be removed through normalization by the expected power at various spatial positions.

A. Long Data Window and Observation Interval

Wideband Point MLE: A 3-D plot of distance, velocity, and receiver output for the wideband point MLE is shown in Fig. 15 with a tapered data window of 30 periods, and with a tapered data window of 50 periods in Fig. 16. In each case, the observation window is rectangular and 384 periods in length, and therefore individual estimates are averaged over the entire data set.

For regions of uniform velocity, the resolution of the estimate improves with the increase in data window as reported in Section IV-C. The slope of the velocity distribution near the peak velocity increases as the data window is increased. This was specifically shown in Fig. 13 but can also be observed in Figs. 15 and 16. In addition, near the vessel wall, the resolution improves and the true velocity distribution becomes clearer. The high amplitude scattering of the vessel wall at a velocity near 0 m/s becomes distinct from the actual velocity of the moving scatterers within this region.

As expected for this laminar flow condition, a smooth change in the mean velocity and the velocity spread as a function of spatial position can be observed. We also observe that the maximum likelihood velocity approximates a parabolic profile, and the computed mean in each position also will be shown in Section VIII to approximate a parabolic profile. An indicator of velocity spread, the maximum amplitude of the receiver output is shown to increase significantly as the center of the vessel is approached, with its uniform velocity.

It was expected that the reliability of the averaged estimate would decrease as the ratio of the data window to the observation window decreases below an order of magnitude. Since a total of 384 vectors of data are available, the estimator reliability is predicted to decrease for data windows above 38 periods. In Fig. 16, the variance of the amplitude of the estimator output has increased, as expected.

Wideband Range Spread MLE: Fig. 17 shows the experimental output of the wideband range spread MLE using a raised cosine data window of 35 periods and a rectangular observation window of 384 periods. The resolution of the wideband range spread MLE is suprerior to the wideband point MLE. Although this is shown more clearly in the 2-D resolution plot, the width of the main resolution lobe of the wideband range spread MLE is smaller than the mainlobe using the wideband point MLE and an equivalent data window.

In addition, the magnitude of the range spread MLE receiver output and the signal to noise ratio is larger than comparable quantities for the wideband point MLE. The exact change in the signal to noise ratio depends upon the window chosen in the estimator.

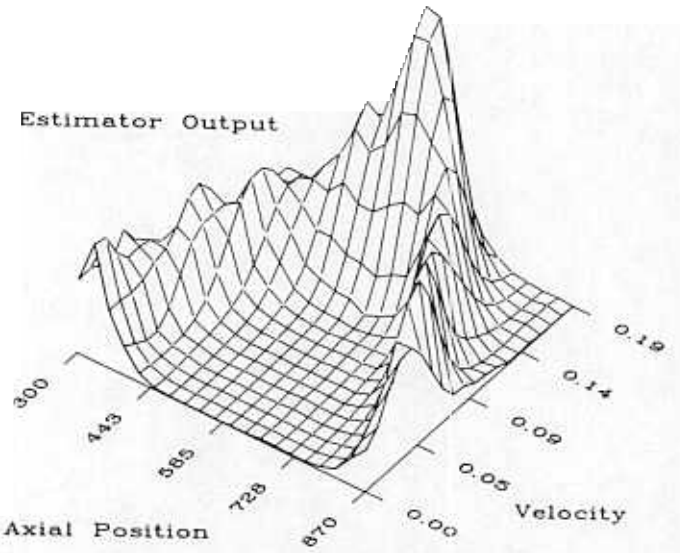

Fig. 17. Three-dimensional display of wideband range spread MLE, raised cosine data window of 35 periods, as a function of the indexed axial position and velocity in m/s.

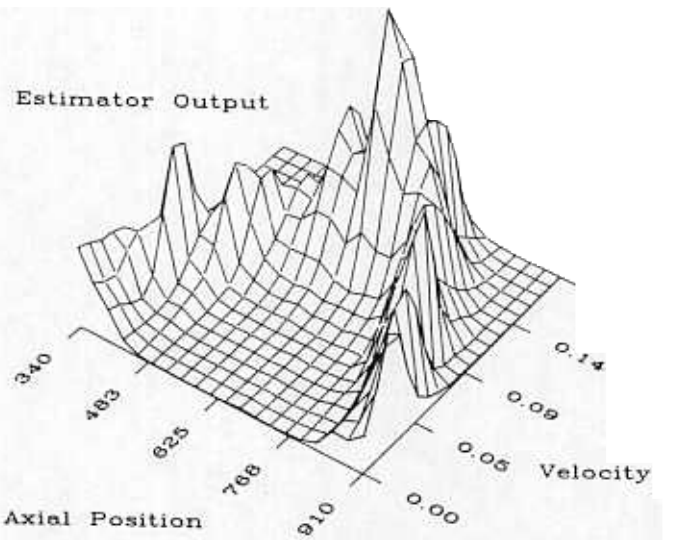

Fig. 18. Three-dimensional display of narrowband MLE, data window of 35 periods, as a function of the indexed axial position and velocity in m/s

Narrowband MLE: Fig. 18 shows the output of the narrowband MLE for a data window of 35 periods and rectangular observation window of 384 periods. This three dimensional plot of the narrowband ML velocity estimate, averaged over all of the data, shows more randomness than the wideband MLE. The amplitude becomes erratic as the velocity increases. Due to the variation in estimator performance as a function of absolute velocity, the amplitude and width of the velocity distribution in individual spatial bins lose significance.

B. A Single Velocity Estimate

Wideband Range Spread MLE: A single wideband range spread estimate is shown in Fig. 19, using a data window of 35 periods. The amplitude of the receiver output for the spread velocity components near the vessel wall has decreased significantly and, although not shown, varies significantly between individual estimates. The use of a single data window without the averaging of subsequent estimates has produced an increased variance in the amplitude of the receiver output.

Narrowband MLE: A single narrowband ML estimate, using a data window of 35 periods, is shown in Fig. 20. It shows a very high level of noise and, in comparison with the wideband ML estimator, the computed variance is much higher. Using the narrowband MLE, it is the limited transit time of scatterers through the sample volume that increases the variance. Once again, the performance difference verifies the ability of the wideband MLE to track groups of scatterers.

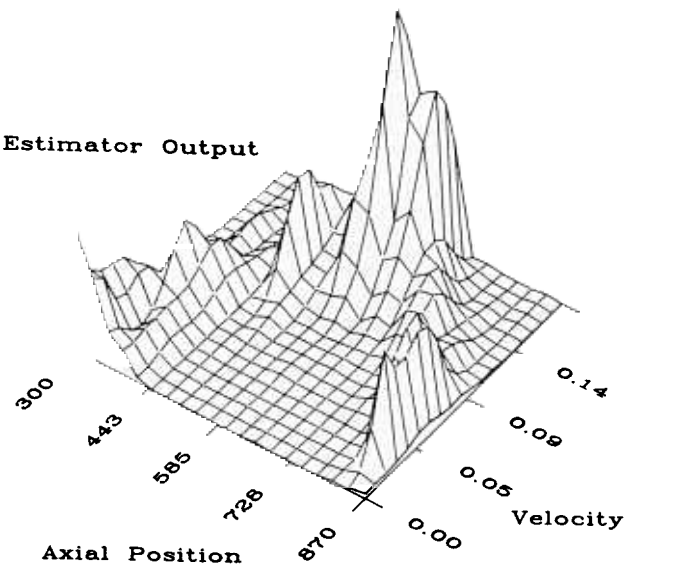

Fig. 19. Three-dimensional display of single wideband range spread estimate, raised cosine data window of 35 periods, as a function of the indexed axial position and velocity in m/s.

VIII. The Estimation of Mean Velocity

The mean velocity profile across the vessel was also computed for the wideband point MLE and the narrowband MLE using 35 period data windows. The mean velocity is plotted in Fig. 21. The mean of the wideband point MLE produces a parabolic profile with a maximum of approximately 0.16 m/s. The expected mean in the center of the vessel, based on the volume flow estimate and the spatial sample volume size, was 0.167 m/s. The experimental error in the volume flow estimate calculated by Embree [1] was 0.7%. The combined potential experimental error from vessel size estimation, vessel expansion, angle measurement, and volume flow estimation may account for this discrepancy. We observe that the narrowband MLE output at higher velocities is inconsistent with the expected flow, given the experimental conditions.

The average standard deviation of the mean velocity estimate using the wideband point MLE was approximately 0.0035 m/s for velocities above 0.125 m/s, and the average for the narrowband MLE was approximately 0.0055 m/s. The performance of the narrowband MLE and wideband point MLE are nearly equivalent for low velocity scatterers, as predicted in Part I. The standard deviation at low velocities is approximately 0.007 m/s. This increase in the standard deviation of the mean velocity estimate for both MLEs is due to the presence of a velocity spread target and was predicted in the derivation of the bound on the variance. It was shown in Part I that the variance of the estimate of the mean velocity was proportional to the width of the velocity distribution within the sample volume.

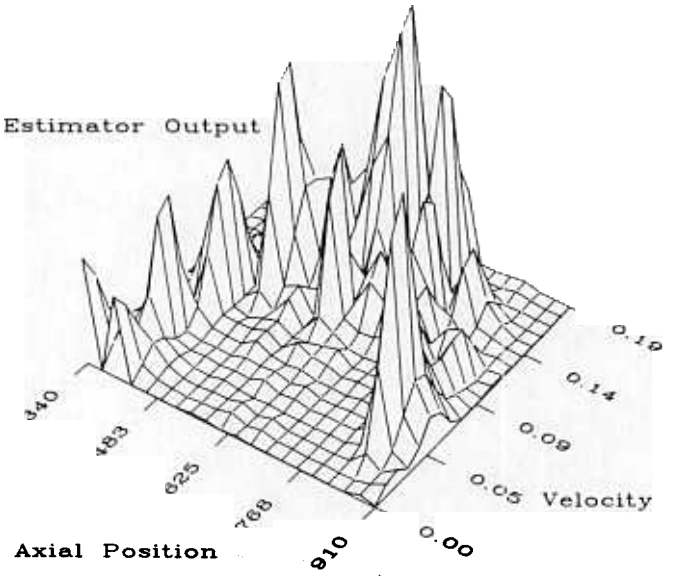

Fig. 20. Three-dimensional display of single narrowband estimate, data window of 35 periods, as a function of the indexed axial position and velocity in m/s.

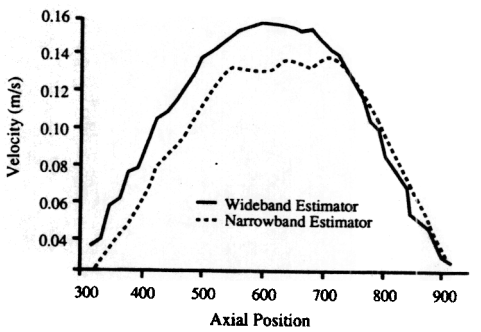

Fig. 21. Experimental mean velocity estimates using wideband point MLE and narrowband MLE, for each indexed axial position.

Therefore, it would be expected to increase near the vessel wall due to the increased spread within the sample volume.

IX. Conclusion

The ultrasonic data analyzed in this paper confirmed experimentally the theoretical models and analyses of Part I. The form of the averaged correlation demonstrated that the correlation envelope, in addition to the phase, can be used to estimate the velocity of scatterers. It also confirmed that the shape of the correlation function conveys information regarding the velocity distribution within the sample volume, as expected.

The analysis demonstrated that the wideband ML estimation strategies offer an improvement over narrowband velocity estimation. The predicted *improvement in velocity resolution* has been demonstrated, as well as the *reduction in the height of subsidiary velocity peaks*. The estimator resolution improvement consists of a decrease in the overall width of the mainlobe and an improvement in the local accuracy of the estimator. The wideband range spread MLE was shown to offer additional improvement in velocity resolution. An important advantage of both wideband strategies is the considerably higher transmitted signal power that can be used with a short wideband signal, thus improving the signal to noise level of the estimate of velocity in a small sample volume.

By the use of these estimation strategies, the mean velocity and velocity distribution can be estimated for each spatial location within the vessel. Therefore, the improved model for acoustic scattering by blood, together with generalized signal processing schemes, can improve the spatial mapping of scatterer velocity and the quality of the velocity estimate. This information can be effectively presented through the use of a three dimensional spatial-velocity profile display. Complete information regarding the spatial-velocity profile throughout the vessel can thus be presented simultaneously.

Acknowledgment

The authors wish to thank Dr. William O'Brien, Dr. Paul Embree, Ilmar Hein and the University of Illinois Bioacoustics Center for the experimental data used in this paper.

References

[1] P. M. Embree, and W. T. Mayo, "Ultrasonic M-Mode RF display technique with application to flow visualization," *SPIE Int. Symp. Pattern Recog. Acoust. Imaging*, vol. 768, 1987.

[2] K. W. Ferrara, "Wideband strategies for blood velocity estimation using ultrasound," Ph.D. Dissertation, Univ. Calif., Davis, CA, 1989.

[3] Mani Azimi and A. C. Kak, "An analytical study of Doppler ultrasound systems," *Ultrason. Imaging*, vol. 7, pp. 1-48, 1985.

[4] K. K. Shung, Y. W. Yuan, and D. Y. Fei, "Effect of flow disturbance on ultrasonic backscatter from blood," *J. Acoust. Soc. Amer.*, vol. 75, no. 4, pp. 1265-1272, Apr. 1984.

[5] Y. W. Yuan and K. K. Shung, "Further studies on ultrasonic scattering from blood," in *Proc. 1984 Ultrason. Symp.*, pp. 666-668.

[6] L. Mo and R. Cobbold, "A stochastic model of the backscattered Doppler ultrasound from blood," *IEEE Trans. Biomed. Eng.*, vol. BME-33, no. 1, pp. 20-27, Jan. 1986.

[7] L. Hatle and B. Angelsen, *Doppler Ultrasound in Cardiology*. Philadelphia: Lea and Febiger, 1985.

[8] C. Kasai and K. Namekawa, "Real-time two-dimensional Doppler flow mapping using ultrasound doppler," *Recent Advances in Ultrasound Diagnosis 5*, A. Kurjak, G. Kossoff, Eds. New York: Elsevier, 1986.

[9] K. W. Ferrara and V. R. Algazi, "A new wideband spread target maximum likelihood estimator for blood velocity estimation—Part I: Theory," *IEEE Trans. Ultrason. Ferroelec. Freq. Contr.*, vol. 38, no. 1, pp. 1-16, Jan. 1991.

Katherine W. Ferrara (M'87), for a photograph and biography, please see page 16 of this Transactions.

V. Ralph Algazi (M'58-SM'84), for a photograph and biography please see page 16 of this Transactions.